JOURNAL OF MATERIALS SCIENCE 18 (1983) 2260–2268

Thermoelastic analysis of hybrid fabric composites

TAKASHI ISHIKAWA*, TSU-WEI CHOU
Department of Mechanical and Aerospace Engineering, University of Delaware, Newark, Delaware 19711, USA

This paper examines the thermoelastic behaviour of hybrid fabric composites. The analysis is based upon modifications of the "fibre undulation model" and "bridging model" originally developed by the authors for non-hybrid fabric composites. Predictions of elastic stiffness constants as well as in-plane thermal expansion and thermal bending coefficients of hybrids have been made. Numerical results compare very favourably with the limited experimental data available.

1. Introduction

The mechanical behaviour of fabric-reinforced composite materials has received the increasing attention of researchers recently [1–5]. The thermoelastic properties of non-hybrid fabric composites has been studied by Ishikawa [6] and Ishikawa and Chou [7–9] in a series of papers. In the case of hybrid fabric composites, Ishikawa and Chou [10] presented a theoretical prediction of the upper and lower bounds of elastic constants based upon a "mosaic model", originally developed by Ishikawa [6]. A considerable effort was also made [10] to identify and categorize the various combinations of fibre materials and geometrical patterns in hybrid fabrics. Although [10] provides a convenient means of estimation of the elastic properties of hybrids, the upper and lower bound predictions are rather far apart.

The purpose of the present paper is to provide an improved analysis of the thermoelastic properties of hybrid fabric composites. The basic analytical tools are the "fibre undulation model" and "bridging model" developed by the authors [7, 8]. Both models have been modified here to fit the situation of hybrid fabric structures. Numerical results of the analysis have been compared with the experimental work of Zweben and Norman [1].

The identification and categorization of fabric structures are made based upon the geometrical as well as material repeating pattern in the warp and fill directions. Two geometrical quantities are necessary: a fill thread is interlaced with every n_{wg}th warp thread, and a warp thread is interlaced with every n_{fg}th fill thread. Here, the subscripts f and w denote the fill and warp threads, respectively; g signifies a geometrical parameter. This paper is restricted to the case of $n_g = n_{fg} = n_{wg}$. Consider the case that the fabric is composed of two kinds of fibre materials denoted by α and β. Two material parameters are defined: the pattern of arrangement of fibre types in the filling direction repeats for every n_{fm} warp thread, and the pattern of fibre types in the warp direction repeats for every n_{wm} filling thread. The subscript m indicates a material parameter. Fig. 1 demonstrates a hybrid fabric with homogeneous interlacing for $n_g = 8$, $n_{fm} = 4$ and $n_{wm} = 4$. It is also noted that for a given n_{fm} value the number of α and β threads are denoted by n^{α}_{fm} and n^{β}_{fm}, respectively. Similarly, n^{α}_{wm} and n^{β}_{wm} denote the number of α and β threads for a given n_{wm} value.

Throughout this paper, we specify $n_g = 8$ and the fibre material repeating parameters (n^{α}_{fm}, n^{β}_{fm}, n^{α}_{wm}, n^{β}_{wm}) are of the three types: (3, 1; 3, 1), (1, 1; 1, 1) and (1, 3; 1, 3). Also homogeneous interlacing [10] is assumed in the analysis. These conditions are chosen to coincide with the systems of Zweben and Norman [1] and the authors [10]. Furthermore, the systems of

*On leave from National Aerospace Laboratory, 1880 Jindaiji, Chofu, Tokyo 182, Japan.

0022–2461/83 $03.00 + .12

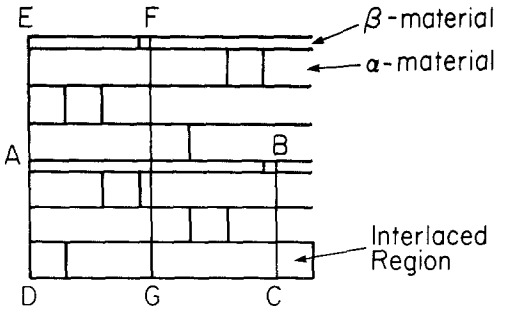

Figure 1 A hybrid fabric with homgeneous interlacing, for $n_g = 8$, $n_{fm} = n_{wm} = 4$, α and β indicate two types of thread materials. ABCD and EFGD denote two choices of repeating units.

(3, 1; 3, 1) and (1, 3; 1, 3) are interchangeable by interchanging the α and β materials. Therefore, only the systems of (3, 1; 3, 1) and (1, 1; 1, 1) will be considered here.

2. Fundamentals of analysis

The first theoretical basis of the present work is the classical laminated plate theory [11, 12]. The constitutive equations including thermal terms for a cross-ply laminate are

$$\begin{aligned} N_i &= A_{ij}^{\xi\eta}\epsilon_j^0 + B_{ij}^{\xi\eta}\kappa_j - \Delta T\tilde{A}_i^{\xi\eta} \\ M_i &= B_{ij}^{\xi\eta}\epsilon_j^0 + D_{ij}^{\xi\eta}\kappa_j - \Delta T\tilde{B}_i^{\xi\eta} \end{aligned} \tag{1a}$$

where

$$(\tilde{A}_i^{\xi\eta}, \tilde{B}_i^{\xi\eta}) = \int_{-h/2}^{h/2} (1, z) q_i^{(k)} \mathrm{d}z \tag{1b}$$

and

$$q_i^{(k)} = Q_{ij}^{(k)}\alpha_j^{(k)}. \tag{1c}$$

Here, the definitions of force resultant, N_i, moment resultant, M_i, extensional stiffness, A_{ij}, coupling stiffness, B_{ij}, bending stiffness, D_{ij}, plate mid-plane strain, ϵ_j^0 and curvature, κ_j, and reduced stiffness, Q_{ij}, have been given by Jones [11]. Also, ΔT is a small uniform temperature change, and α_j denotes a thermal expansion coefficient. The integration of Equation 1b is carried out through the plate thickness, h, and k stands for one of the ξ and η fibre materials or the matrix. Equation 1a can be inverted to give

$$\begin{aligned} \epsilon_i^0 &= \tilde{a}_{ij}^{*\xi\eta}N_j + b_{kj}^{*\xi\eta}M_j + \Delta T\tilde{a}_i^{*\xi\eta} \\ \kappa_i &= b_{ij}^{*\xi\eta}N_j + d_{ij}^{*\xi\eta}M_j + \Delta T\tilde{b}_i^{*\xi\eta} \end{aligned} \tag{2a}$$

where

$$\begin{aligned} \tilde{a}_i^{*\xi\eta} &= a_{ij}^{*\xi\eta}\tilde{A}_j^{\xi\eta} + b_{ij}^{*\xi\eta}\tilde{B}_j^{\xi\eta} \\ \tilde{b}_i^{*\xi\eta} &= b_{ij}^{*\xi\eta}\tilde{A}_j^{\xi\eta} + d_{ij}^{*\xi\eta}\tilde{B}_j^{\xi\eta}. \end{aligned} \tag{2b}$$

Here $a_{ij}^{*\xi\eta}$, $b_{ij}^{*\xi\eta}$ and $d_{ij}^{*\xi\eta}$ in Equation 2a are the compliance constants; $\tilde{a}_i^{*\xi\eta}$ and $\tilde{b}_i^{*\xi\eta}$ denote respectively, the in-plane thermal expansion coefficient and thermal bending coefficient.

The second theoretical basis of the present analysis is the one-dimensional physical model known as the "fibre undulation model" [7, 8], which takes into account fibre continuity. The original approach of our work [7, 8] has been modified slightly here to allow the variation in thread width between the two kinds of fibre material in the hybrid fabric. Sectional shapes of some typical interlacing regions are shown in Figs. 2a and b. Here, the thread width ratio, r, is defined by

$$r = a_\beta/a_\alpha \tag{3}$$

where a_α and a_β denote the width of the α and β threads, respectively. Since a_α is used as a basis of measurement for thread, the notation $a = a_\alpha$ will be used from here on. Also, in Fig. 2, a_u denotes the length of undulation of a fill thread when it is interlaced with an α warp thread. Points a_0 and a_1 are the ends of the undulated portion of the threads along the fill direction.

The sinusoidal type of functions used previously [7] for describing the undulation shapes are preserved here. For the case where the warp thread is composed of α material (Fig. 2a), the height of the fill thread is given by

$$h_1^\alpha(x) = \begin{cases} 0 & (0 \leqslant x \leqslant a_0) \\ \left\{1 + \sin\left[\left(x - \dfrac{a}{2}\right)\dfrac{\pi}{a_u}\right]\right\}\dfrac{h_t}{4} & (a_0 \leqslant x \leqslant a_1). \end{cases} \tag{4}$$

When the warp thread is composed of β material, the height of the fill thread is given by

$$h_1^\beta(x) = \begin{cases} 0 & (0 \leqslant x \leqslant ra_0) \\ \left\{1 + \sin\left[\left(x - \dfrac{ra}{2}\right)\dfrac{\pi}{ra_u}\right]\right\}\dfrac{h_t}{4} & \\ & (ra_0 \leqslant x \leqslant ra_1) \end{cases} \tag{5}$$

where h_t denotes the total thickness of threads (see Fig. 2).

Corresponding to the cases of Equations 4 and 5, the heights of the warp threads are given,

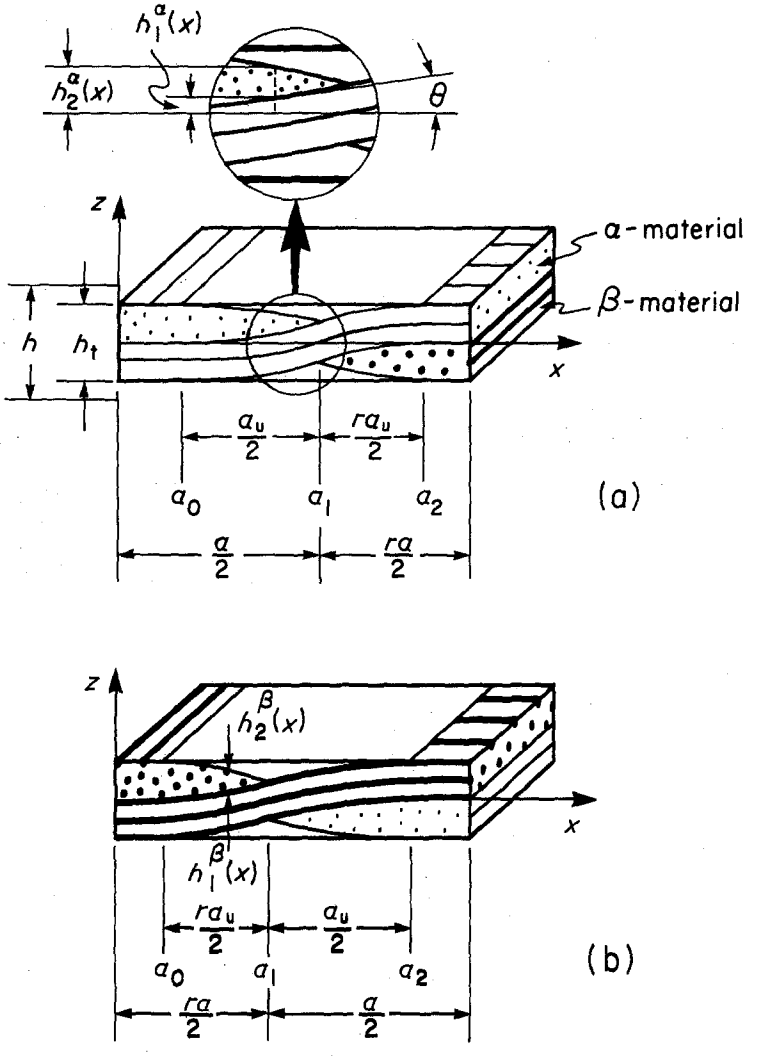

Figure 2 Typical structures of interlaced regions of hybrid fabric composites. h denotes plate thickness and $h-h_t$ indicates the total thickness of pure matrix layers. $a = a_\alpha$. (a) fill: α material; warp: α or β material. (b) fill: β material; warp: α or β material.

respectively, by

$$h_2^\alpha(x) = \begin{cases} h_t/2 & (0 \leqslant x \leqslant a_0) \\ \left\{1 - \sin\left[\left(x - \frac{a}{2}\right)\frac{\pi}{a_u}\right]\right\}\frac{h_t}{4} & \\ (a_0 \leqslant x \leqslant a_1) & \end{cases} \quad (6)$$

$$h_2^\beta(x) = \begin{cases} h_t/2 & (0 \leqslant x \leqslant ra_0) \\ \left\{1 - \sin\left[\left(x - \frac{ra}{2}\right)\frac{\pi}{ra_u}\right]\right\}\frac{h_t}{4} & \\ (ra_0 \leqslant x \leqslant ra_1). & \end{cases} \quad (7)$$

It should be noted that Equations 4 to 7 are written for the portion of the undulated region where the fill thread is beneath the warp thread.

A key assumption made in the fibre undulation model [7, 8] is that the classical laminated plate theory is applicable to each infinitesimal slice of material of width dx. Then the local plate extensional stiffness coefficients for the portion where the warp thread is composed of α material, are given by

$$A_{ij}^{\xi\alpha}(x) = Q_{ij}^{M}\left(h - \frac{h_t}{2} + h_1^\alpha(x) - h_2^\alpha(x)\right) + Q_{ij}^{F\xi}(x)\frac{h_t}{2} + Q_{ij}^{W\alpha}(h_2^\alpha(x) - h_1^\alpha(x)) \quad (8)$$

where the superscripts F, W, and M denote the fill thread region, warp thread region, and pure matrix material, respectively, ξ stands for α or β material, and h denotes the total laminate thickness, including the pure matrix layers. Furthermore, the first superscript of A_{ij} indicates the fill material and the second one the warp material. This convention is followed for all the stiffness and compliance constants throughout this paper.

Likewise, for the portion of the laminate in Fig. 2b where the warp thread is composed of β material,

$$A_{ij}^{\xi\beta}(x) = Q_{ij}^{M}\left(h - \frac{h_t}{2} + h_1^{\beta}(x) - h_2^{\beta}(x)\right) + Q_{ij}^{F\xi}(x)\frac{h_t}{2} + Q_{ij}^{W\beta}(h_2^{\beta}(x) - h_1^{\beta}(x)). \quad (9)$$

Similarly, expressions for $B_{ij}^{\xi\alpha}(x)$, $B_{ij}^{\xi\beta}(x)$, $D_{ij}^{\xi\alpha}(x)$ and $D_{ij}^{\xi\beta}(x)$ can also be obtained.

The local thermal deformation coefficients can be obtained by replacing Q_{ij} in Equation 9 by q_i (Equation 1c). For instance,

$$\tilde{A}_i^{\xi\alpha}(x) = q_i^{M}\left(h - \frac{h_t}{2} + h_1^{\alpha}(x) - h_2^{\alpha}(x)\right) + q_i^{F\xi}(x)\frac{h_t}{2} + q_i^{W\alpha}(h_2^{\alpha}(x) - h_1^{\alpha}(x)). \quad (10)$$

Explicit expressions of off-axis properties in the fill thread region, $Q_{ij}^{F\xi}(x)$ and $q_i^{F\xi}(x)$ are given elsewhere [7–9]. Local compliance constants $a_{ij}^{*\xi\alpha}(x)$, $b_{ij}^{*\xi\alpha}(x)$ and $d_{ij}^{*\xi\alpha}(x)$ are obtained by inverting $A_{ij}^{\xi\alpha}(x)$, $B_{ij}^{\xi\alpha}(x)$ and $D_{ij}^{\xi\alpha}(x)$. Similarly, $a_{ij}^{*\xi\beta}(x)$, $b_{ij}^{*\xi\beta}(x)$ and $d_{ij}^{*\xi\beta}(x)$ are obtained from $A_{ij}^{\xi\beta}(x)$, $B_{ij}^{\xi\beta}(x)$ and $D_{ij}^{\xi\beta}(x)$. Finally, the thermal coefficients $\tilde{a}_i^{*\xi\alpha}$, $\tilde{b}_i^{*\xi\alpha}$, $\tilde{a}_i^{*\xi\beta}$ and $\tilde{b}_i^{*\xi\beta}$ can be obtained from Equation 2b.

Consider again the one-dimensional idealized model of a hybrid laminate. The average extensional compliance for the portion containing α warp threads is defined as

$$\bar{a}_{ij}^{*U\xi\alpha} = \frac{2}{a}\int_0^{a/2} a_{ij}^{*\xi\alpha}(x)\,dx = \left(1 - \frac{a_u}{a}\right)a_{ij}^{*\xi\alpha} + \frac{2}{a}\int_{a_0}^{a_1} a_{ij}^{*\xi\alpha}(x)\,dx. \quad (11)$$

For the case of β warp threads,

$$\bar{a}_{ij}^{*U\xi\beta} = \left(1 - \frac{a_u}{a}\right)a_{ij}^{*\xi\beta} + \frac{2}{ra}\int_{ra_0}^{ra_1} a_{ij}^{*\xi\beta}(x)\,dx. \quad (12)$$

The superscript U in Equations 11 and 12 signifies the fibre undulation model. Other averaged compliance constants $\bar{b}_{ij}^{*U\xi\alpha}$, $\bar{b}_{ij}^{*U\xi\beta}$, $\bar{d}_{ij}^{*U\xi\alpha}$ and $\bar{d}_{ij}^{*U\xi\beta}$ can be obtained in a similar manner. Expressions of the averaged in-plane thermal expansion coefficients can be obtained from Equations 11 and 12 by replacing a_{ij}^{*} by the appropriate $\tilde{a}_i^{*}$. Also, the thermal bending coefficients can be easily obtained. However, it should be noted that $\bar{b}_{ij}^{*U\xi\eta}$ and $\bar{\tilde{b}}_i^{*U\xi\eta}$ do not vanish when the integrations in Equations 11 and 12 are carried out over the entire length of $a/2$ $[(1+r)]$ (Fig. 2), unlike the cases of [7, 9] for non-hybrid fabrics. This fact is caused by the differences in thread widths and properties of the constituent fibres of the fabric. Finally, the averaged stiffness constants $\bar{A}_{ij}^{U\xi\eta}$, $\bar{B}_{ij}^{U\xi\eta}$ and $\bar{D}_{ij}^{U\xi\eta}$ can be obtained by inverting these averaged compliance constants. Then the averaged thermal constants $\bar{\tilde{A}}_i^{U\xi\eta}$ and $\bar{\tilde{B}}_i^{U\xi\eta}$ are obtained from the inverted form of Equation 2b. It should be noted that the thermoelastic constants derived in this paper are based upon the definition of $h_1(x)$ and $h_2(x)$ given in Equations 4 and 5: the fill thread is situated beneath the warp thread. Thus the coupling stiffness constants for the right hand portions of Figs. 2a and 2b, for instance, are denoted by $-\bar{B}_{ij}^{U\alpha\beta}$ and $-\bar{B}_{ij}^{U\beta\alpha}$, respectively.

3. Bridging model analysis – (3,1;3,1) case

3.1. Repeating region ABCD of Fig. 1

The case of fabrics with $n_g = 8$, $(n_{fm}^{\alpha}, n_{fm}^{\beta}; n_{wm}^{\alpha}, n_{wm}^{\beta}) = (3,1;3,1)$ and homogeneous interlacing pattern is considered first. A possible shape of the minimum repeating unit is indicated in Fig. 1 as the area ABCD. The three-dimensional view of this repeating unit showing the interlaced configurations of the α and β threads is given in Fig. 3, which consists of five regions, R_1, R_2, R_3, R_4 and R_5, arranged in series along the loading direction. However, other choices of the division of regions are possible. It is assumed in the following analysis that the resultant force in the loading direction of every region is identical.

To exemplify the analysis of the bridging model, region R_2 is considered. Region 2 consists of four sub-regions labelled R_2^1, R_2^2, R_2^3 and R_2^4 (see Fig. 4). The averaged strains of the sub-regions are also assumed to be identical. The averaged compliance constants of regions R_2^1 and R_2^2 are the same and are given by

$$\bar{p}_{ij}^{*}(R_2^1) = \frac{1}{3+r}(3p_{ij}^{*\alpha\alpha} + rp_{ij}^{*\alpha\beta}) \quad (13)$$

where p stands for a, b or d, and the constants $a_{ij}^{*\xi\eta}$, $b_{ij}^{*\xi\eta}$ and $d_{ij}^{*\xi\eta}$ are defined in Equations 2a and 2b. The region R_2^4 also has straight threads and

$$\bar{p}_{ij}^{*}(R_2^4) = \frac{1}{3+r}(3p_{ij}^{*\beta\alpha} + rp_{ij}^{*\beta\beta}). \quad (14)$$

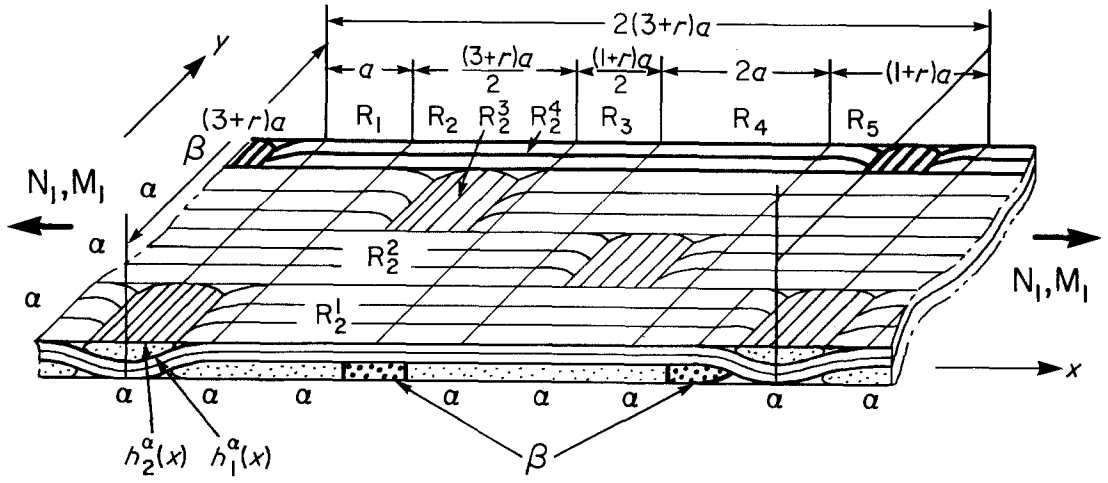

Figure 3 A bridging model for $n_g = 8$ and the (3,1;3,1) case (region ABCD of Fig. 1).

From the undulated portion R_2^3, the following relation is only valid for the constants a and d:

$$\bar{p}_{ij}^{*U}(R_2^3) = \frac{1}{3+r}(3\bar{p}_{ij}^{*U\alpha\alpha} + r\bar{p}_{ij}^{*U\alpha\beta}) \quad (15)$$

where the process by which $\bar{p}_{ij}^{*U}$ is obtained has been given in Section 2. In the case of coupling constants

$$\bar{b}_{ij}^{*U}(R_2^3) = \frac{1}{3+r}(\bar{b}_{ij}^{*U\alpha\alpha} - r\bar{b}_{ij}^{*U\alpha\beta}). \quad (16)$$

The reason for the minus sign in Equation 16 has been explained at the end of Section 2.

The averaged stiffness constants of each sub-region are obtained by inverting the corresponding compliance constants of Equations 13 to 16. Based upon the assumption of iso-strain condition in each region, the averaged stiffness of an entire region can be determined. For example, the averaged extensional stiffness of region R_2 is given by

$$\bar{A}_{ij}(R_2) = \frac{1}{3+r}(2\bar{A}_{ij}(R_2^1) + \bar{A}_{ij}^{U}(R_2^3) + r\bar{A}_{ij}(R_2^4). \quad (17)$$

Similar expressions can be written for $\bar{B}_{ij}(R_2)$ and $\bar{D}_{ij}(R_2)$. By inverting $\bar{A}_{ij}(R_2)$, $\bar{B}_{ij}(R_2)$ and $\bar{D}_{ij}(R_2)$, expressions of $\bar{a}_{ij}^{*}(R_2)$, $\bar{b}_{ij}^{*}(R_2)$ and $\bar{d}_{ij}^{*}(R_2)$ can be obtained.

For the fabric composite of Fig. 3, it is assumed that each region, R_1, R_2, R_3, R_4 or R_5 carries the same load N_1. Thus the compliance constants of the entire composite can be regarded as the volume average of the compliances of the individual regions:

$$\bar{p}_{ij}^{*HS} = [3\bar{p}_{ij}^{*}(R_1) + \frac{3+r}{2}\bar{p}_{ij}^{*}(R_2) + \frac{(1+r)}{2}\bar{p}_{ij}^{*}(R_3) + (1+r)\bar{p}_{ij}^{*}(R_5)]/(6+2r) \quad (18)$$

where, the superscript HS indicates hybrid satin composites, and $\bar{p}_{ij}^{*}(R_1) = \bar{p}_{ij}^{*}(R_4)$. The inversion of $\bar{p}_{ij}^{*HS}$ constants gives the stiffness coefficients of the entire composite, $\bar{A}_{ij}^{HS}$, $\bar{B}_{ij}^{HS}$ and $\bar{D}_{ij}^{HS}$. The basic idea of analysis presented above is identical to that of the "bridging model" first proposed in [8], in which only non-hybrid fabric composites were considered.

The derivation of the thermal coefficients of the composite model shown in Fig. 3 is briefly outlined below. In region R_2, the local thermal coefficients for the sub-regions R_2^1 and R_2^4 can be

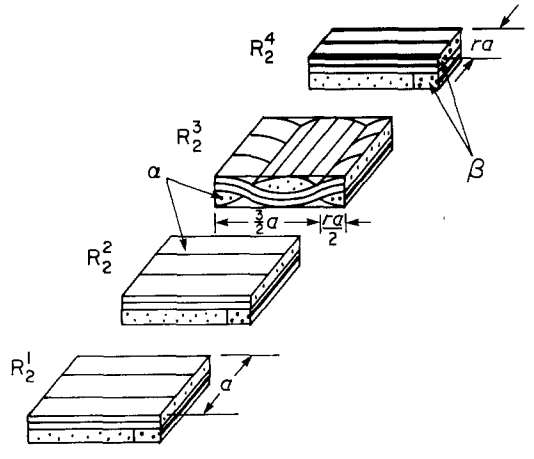

Figure 4 Detail view of region R_2 in Fig. 3.

obtained by replacing p_{ij}^* of Equations 13 and 14 by $\tilde{p}_i^*$ where $\tilde{p}_i^*$ stands for thermal expansion coefficient, $\tilde{a}_i^*$, or thermal bending coefficient, $\tilde{b}_i^*$. For sub-regions R_2^3, $\bar{a}_{ij}^{*U}$ in Equation 15 is replaced by $\tilde{a}_i^{*U}$ and $\bar{b}_{ij}^{*U}$ in Equation 16 is replaced by $\tilde{b}_i^{*U}$. As to the region R_2, the averaged thermal constants $\bar{\bar{A}}_i(R_2^1), \bar{\bar{A}}_i(R_2^2), \bar{\bar{A}}_i(R_2^3), \bar{\bar{A}}_i(R_2^4)$ and $\bar{\bar{B}}_i(R_2^1) \ldots \bar{\bar{B}}_i(R_2^4)$ can be obtained by inverting Equation 2b. Then, by following the bridging model approach for thermal constants [9] and by adopting the iso-strain assumption for region R_2, we obtain

$$\begin{bmatrix} \bar{A}_{ij}(R_2) & \bar{B}_{ij}(R_2) \\ \bar{B}_{ij}(R_2) & \bar{D}_{ij}(R_2) \end{bmatrix} \begin{Bmatrix} \bar{\epsilon}_j^0(R_2) \\ \bar{\kappa}_j(R_2) \end{Bmatrix}$$

$$= \Delta T \left[2 \begin{Bmatrix} \bar{\bar{A}}_i(R_2^1) \\ \bar{\bar{B}}_i(R_2^1) \end{Bmatrix} + \begin{Bmatrix} \bar{\bar{A}}_i^U(R_2^3) \\ \bar{\bar{B}}_i^U(R_2^3) \end{Bmatrix} + r \begin{Bmatrix} \bar{\bar{A}}_i(R_2^4) \\ \bar{\bar{B}}_i(R_2^4) \end{Bmatrix} \right] \Big/ (3+r)$$

$$= \Delta T \begin{Bmatrix} \bar{\bar{A}}_i(R_2) \\ \bar{\bar{B}}_i(R_2) \end{Bmatrix} \tag{19}$$

where $\bar{A}_{ij}(R_2)$, $\bar{B}_{ij}(R_2)$ and $\bar{D}_{ij}(R_2)$ are given by Equation 17. Then

$$\begin{Bmatrix} \bar{\bar{a}}_i^*(R_2) \\ \bar{\bar{b}}_i^*(R_2) \end{Bmatrix} = \begin{bmatrix} \bar{a}_{ij}^*(R_2) & \bar{b}_{ij}^*(R_2) \\ \bar{b}_{ij}^*(R_2) & \bar{d}_{ij}^*(R_2) \end{bmatrix} \begin{Bmatrix} \bar{\bar{A}}_j(R_2) \\ \bar{\bar{B}}_j(R_2) \end{Bmatrix}. \tag{20}$$

Finally, expressions of thermal coefficients of the entire hybrid satin composite can be obtained by replacing p_{ij}^* in Equation 18 by $\tilde{p}_i^*$ where p now stands for a or b.

3.2. Repeating region EFGD of Fig. 1

It has been shown [10] that both regions ABCD and EFGD of Fig. 1 can be treated as a repeating region for the entire fabric composite. The derivation of the thermoelastic constants for the repeating region EFGD is outlined below and comparisons of results with those obtained for region ABCD will be given later.

Fig. 5 depicts the three-dimensional view of region EFGD, which is composed of regions R_1, R_2 and R_3. Region R_1 is further divided into eight sub-regions, R_1^1, R_1^2, ..., R_1^8. The compliance constants of each sub-region are again obtained following the derivation of Equations 13 to 16. Then, the averaged stiffness constants of region R_1 are given by

$$\bar{P}_{ij}(R_1) = [2\bar{P}_{ij}(R_1^2) + \bar{P}_{ij}^U(R_1^1) + r\bar{P}_{ij}(R_1^4)]/(3+r) \tag{21}$$

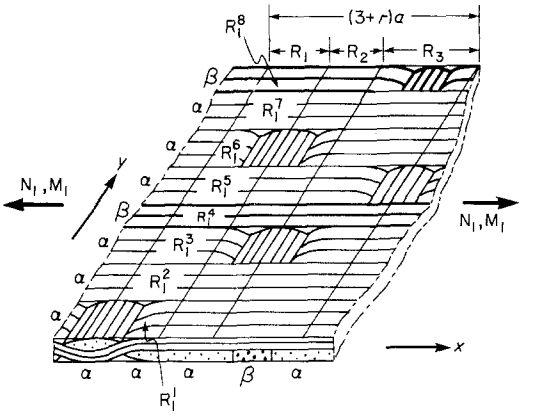

Figure 5 Another bridging model for $n_g = 8$ and the (3,1;3,1) case (region EFGD of Fig. 1).

where

$$\bar{P}_{ij}(R_1^2) = \bar{P}_{ij}(R_1^3) = \bar{P}_{ij}(R_1^5) = \bar{P}_{ij}(R_1^7).$$

Finally, for the entire hybrid satin composites, the compliance constants are given in the general form

$$\bar{p}_{ij}^{*HS} = [2\bar{p}_{ij}^*(R_1) + (1+r)\bar{p}_{ij}^*(R_3)]/(3+r) \tag{22}$$

where the relation $\bar{p}_{ij}(R_1) = \bar{p}_{ij}(R_2)$ has been applied. A procedure parallel to the above can be used to derive the thermal coefficients.

As to the case of (1,3;1,3) material combination, the thermoelastic constants can be derived from the above by simply exchanging the α and β materials.

4. Bridging model analysis – (1,1;1,1) case

This section examines another case of fabric of $n_g = 8$ with homogeneous interlacing and the material repeating parameters of (1,1;1,1). A repeating pattern of the fabric composite is shown in Fig. 6. There are four sub-regions, $R_1^1, \ldots, R_1^4$, in region R_1. It can be shown that

$$\bar{p}_{ij}^*(R_1^2) = \bar{p}_{ij}^*(R_1^4) = (p_{ij}^{*\beta\alpha} + rp_{ij}^{*\beta\beta})/(1+r) \tag{23}$$

$$\bar{p}_{ij}^*(R_1^3) = (p_{ij}^{*\alpha\alpha} + rp_{ij}^{*\alpha\beta})/(1+r) \tag{24}$$

where p stands for a, b or d. For sub-region R_1^1,

$$\left.\begin{aligned} \bar{b}_{ij}^{*U}(R_1^1) &= (\bar{b}_{ij}^{*U\alpha\alpha} - r\bar{b}_{ij}^{*U\alpha\beta})/(1+r) \\ \bar{p}_{ij}^{*U}(R_1^1) &= (\bar{p}_{ij}^{*U\alpha\alpha} + r\bar{p}_{ij}^{*U\alpha\beta})/(1+r). \end{aligned}\right\} \tag{25}$$

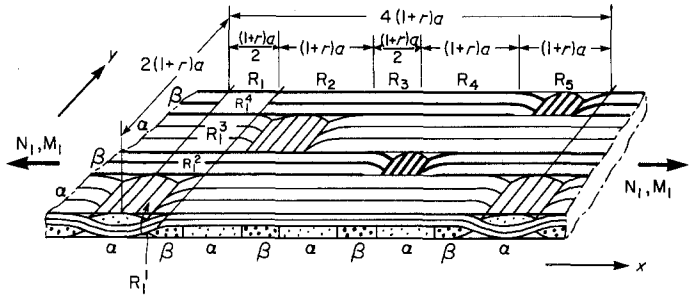

Figure 6 A bridging model for $n_g = 8$ and the (1,1;1,1) case.

Here, p stands for a or d. The stiffness constants for region R_1 are given by

$$\bar{P}_{ij}(R_1) = [\bar{P}^{U}_{ij}(R_1^1) + \bar{P}_{ij}(R_1^3) + 2r\bar{P}_{ij}(R_1^2)]/(2 + 2r). \quad (26)$$

Finally, the compliance constants for the entire fabric composite model are

$$\bar{p}^{*HS}_{ij} = \frac{1}{4(1+r)}\left\{\frac{3}{2}(1+r)\bar{p}^{*}_{ij}(R_1) + \frac{1}{2}(1+r)\bar{p}^{*}_{ij}(R_3) + (1+r)[\bar{p}^{*}_{ij}(R_4) + \bar{p}^{*}_{ij}(R_5)]\right\}. \quad (27)$$

Just as in the case of (3,1;3,1), another repeating unit can be identified for the material repeating parameters of (1,1;1,1). The cases of (3,1;3,1), (1,3;1,3) and (1,1;1,1) give all the possible fibre material combinations for homogeneous interlacing in hybrid fabrics with the present fabric parameters.

5. Numerical results and discussions

Numerical work has been performed to examine the thermoelastic properties of a graphite/Kevlar/epoxy hybrid fabric composite. Basic material properties of unidirectional laminae of graphite/epoxy and Kevlar/epoxy are given in Table I. Most of the values in Table I are estimated from [13–15], based upon the fibre and matrix properties. Because of the lack of experimental data, there is uncertainty in the value of α_T for Kevlar. For all the numerical examples the fibre volume fraction of the unidirectional lamina is assumed to be 65%, which is slightly higher than the total fibre volume fraction of the fabric composite due to the presence of pure matrix layers (Fig. 2a).

Fig. 7 shows the predictions of the extensional stiffness of the present approach as well as those from the bound approach of [10] for a graphite/Kevlar/epoxy system of $n_g = 8$. Three cases of material repeating parameter are presented and the theoretical curves are obtained by changing r continuously. Because values of r far from unity are impractical, cuvres in Fig. 7 are truncated. The present predictions based upon the bridging concept fall in between the upper and lower bounds of [10] and compare very favourably with experiments.

Since the present work modifies the original bridging model for non-hybrid composite of [8], it is worthwhile to compare the predictions of these two slightly different approaches by letting the α and β material be identical in the present analysis. The results, shown in Table II, indicate that the discrepancies in predictions between the non-axial constants (A_{12}, B_{12} and D_{12}) are greater than those for the axial constants (A_{11}, B_{11} and D_{11}). Table III shows that the predictability of the present model is rather insensitive to the selection of repeating unit for a given fabric.

Results of thermal coefficient predictions for the same hybrid system as in Fig. 7 are pre-

TABLE I Thermoleastic properties of the unidirectional laminae, $V_f = 65\%$

Material	E_L(GPa)	E_T(GPa)	ν_L	G_{LT}(GPa)	α_L ($\times 10^{-7}$ °C^{-1})	α_T ($\times 10^{-5}$ °C^{-1})
Graphite/epoxy [10, 13, 14]	132	9.31	0.28	4.61	−2.5	2.7
Kevlar/epoxy [10, 15]	85.3	5.50	0.40	2.54	−11.0	3.2

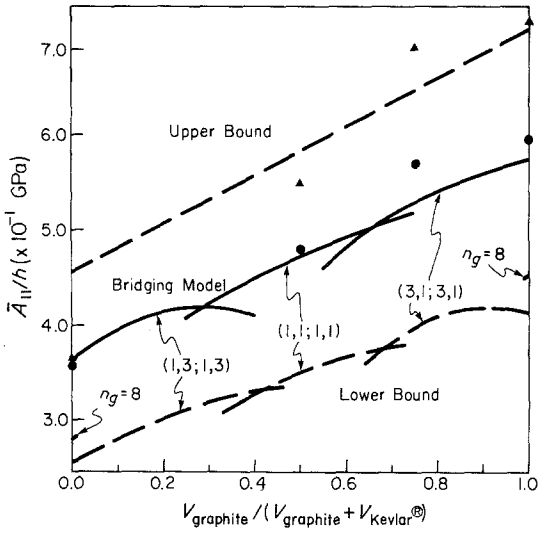

Figure 7 $\bar{A}_{11}/h$ against relative fibre volume fraction of graphite/Kevlar/epoxy composites with $n_g = 8$. ----: bound theory, ——: bridging model, • and ▲: experimental data for fabric and cross-ply laminate composites, respectively. ($h = h_t$, $h/a = 0.4$.)

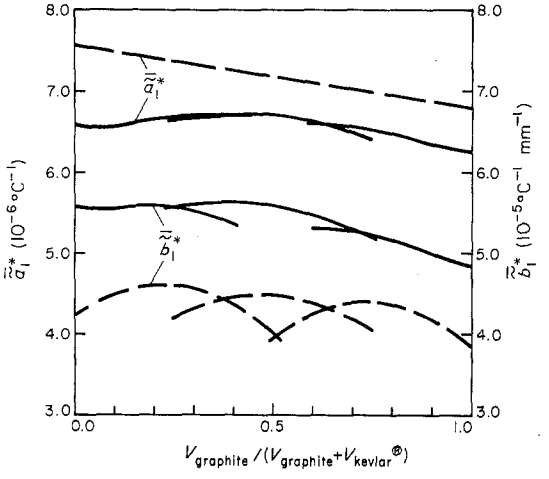

Figure 8 Thermal coefficients against relative fibre volume fraction of graphite/Kevlar/epoxy composites with $n_g = 8$. ---: mosaic model [6], ——: bridging model.

sented in Fig. 8 for the present analysis based upon the bridging model. Also shown in Fig. 8 are predictions based upon the mosaic model and [6]. No experimental data are available for comparison with the theory.

6. Conclusions

1. The one-dimensional fibre undulation concept developed previously has been modified to treat the interlacing of two different types of fibres, and it has been incorporated into a general "bridging model" for predicting thermoelastic properties of hybrid fabric composites.

2. The predictions of elastic stiffness constants compare very favourably with experimental results of graphite/Kevlar/epoxy systems.

3. Theoretical analyses of in-plane thermal expansion and thermal bending coefficients of hybrid fabric composites have also been made.

4. The predicted values of the axial elastic stiffness constants are insensitive to the choice of some possible repeating unit for the fabric material.

TABLE II Comparison of elastic stiffness values of non-hybrid fabric composites ($n_g = 8$) obtained by the present approach and by the method of [8] ($h = h_t = 4.0\,m^{-4}$, $a = a_u = 1.0\,m^{-3}$)

	Present method	Method of [8]
$\bar{A}_{11}$ (MPa m^{-1})	23.21	23.37
$\bar{A}_{12}$	1.009	1.012
$\bar{B}_{11}$ (kN)	1.754	1.796
$\bar{B}_{12}$	-1.405×10^{-3}	-3.456×10^{-4}
$\bar{D}_{11}$ (Nm)	0.2945	0.2973
$\bar{D}_{12}$	1.294×10^{-2}	1.284×10^{-2}

TABLE III Comparisons of elastic stiffness values obtained from two different repeating units for the (3,1;3,1) case ($h = h_t = 4.0\,m^{-4}$, $a = a_u = 1.0\,m^{-3}$)

Relative V_f of α material (%) (r)	89.9 (0.3333)	75 (1.0)	60.3 (2.0)
A_{11} for repeating unit of Fig. 3 (× 10 MPa m^{-1})	2.240	2.113	1.924
A_{11} for repeating unit of Fig. 5 (× 10 MPa m^{-1})	2.207	2.093	1.941

Acknowledgement

This work was supported by the US Army Research Office.

References

1. C. ZWEBEN and J. C. NORMAN, *SAMPE Q.* July (1976) 1.
2. C. ZWEBEN, "Advance Composites: A Revolution for the Designer", American Institute of Aeronautics and Astronautics 50th Annual Meeting "Learn from the Masters" Series, May 1981.
3. I. KIMPARA, A. HAMAMOTO and M. TAKEHANA, *Trans. JSCM,* 3 (1977) 21.
4. J. KAVELKA, "Thermal Expansion of Composites with Canvas-Type Reinforcement and Polymer Matrix", International Conference of Composite Materials 3, Paris, August 1980, p. 770.
5. T. HIRAI and T. SENBA, "On the Mechanical Behavior of Fabric-Strengthened Composites Considering Three-Dimensional Cross-Linked Structure", International Conference of Composite Materials,

3, Paris, August 1980 p. 357.
6. T. ISHIKAWA, *Fibre Sci. Technol.* **15** (1981) 127.
7. T. ISHIKAWA and T. W. CHOU, submitted for publication.
8. *Idem, J. Mater. Sci.* **17** (1982) 3211.
9. *Idem,* submitted for publication.
10. *Idem, J. Compos. Mater.* **16** (1982) 2.
11. R. M. JONES, "Mechanics of Composite Materials" (Scripta, Washington, DC, 1975).
12. J. M. WHITNEY and A. W. LEISSA, *J. Appl. Mech.* **36** (1969) 261.
13. T. ISHIKAWA, K. KOYAMA and S. KOBAYASHI, *J. Compos. Mater.* **11** (1977) 332.
14. *Idem, ibid.* **12** (1978) 153.
15. M. GRUBER and T. W. CHOU, submitted for publication.

Received 18 August
and accepted 2 September 1982